THE JOURNAL OF PHYSICAL CHEMISTRY Letters

pubs.acs.org/JPCL Letter

# Transport Mechanisms Underlying Ionic Conductivity in Nanoparticle-Based Single-Ion Electrolytes

Sanket Kadulkar, Delia J. Milliron, Thomas M. Truskett,* and Venkat Ganesan*

Cite This: J. Phys. Chem. Lett. 2020, 11, 6970−6975 Read Online

ACCESS | Metrics & More | Article Recommendations | Supporting Information

**ABSTRACT:** Recent studies have demonstrated the potential of nanoparticle-based single-ion conductors as battery electrolytes. In this work, we introduce a coarse-grained multiscale simulation approach to identify the mechanisms underlying the ion mobilities in such systems and to clarify the influence of key design parameters on conductivity. Our results suggest that for the experimentally studied electrolyte systems, the dominant pathway for cation transport is along the surface of nanoparticles, in the vicinity of nanoparticle-tethered anions. At low nanoparticle concentrations, the connectivity of cationic surface transport pathways and conductivity increase with nanoparticle loading. However, cation mobilities are reduced when nanoparticles are in close vicinity, causing conductivity to decrease for sufficiently high particle loadings. We discuss the impacts of cation and anion choice as well as solvent polarity within this picture and suggest means to enhance ionic conductivities in single-ion conducting electrolytes based on nanoparticle salts.

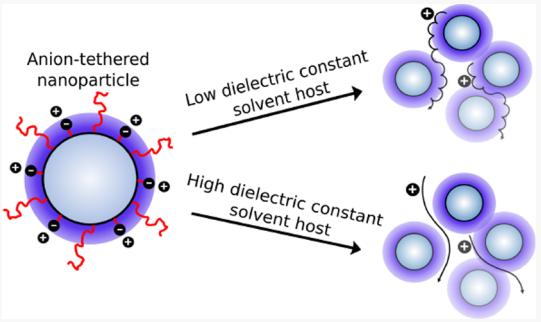


Electrolytes used in lithium-ion batteries are often liquid organic solvents which offer high ionic conductivity.[1] Despite their effective performance, liquid electrolytes present flammability and leakage risks, which limit their applicability.[2] Further, such electrolytes typically exhibit low lithium transference numbers ($t_{Li^+} < 0.5$),[3] which leads to concentration polarization[4] and, when employed with high-capacity lithium metal anodes, dendrite formation.[5] Hence, there is significant interest in developing new electrolyte materials that simultaneously exhibit high conductivity, high $t_{Li^+}$, and desirable safety characteristics.

Nanoparticle-based electrolytes, in which nanoparticles are embedded in ion-conducting solid polymers or liquids, have emerged as a promising platform for achieving high lithium transference numbers.[3] In lithium-salt-doped polymer electrolytes, the addition of nanoparticles has been reported to increase $t_{Li^+}$.[3,6−13] Single-ion conduction ($t_{Li^+} \approx 1$) was recently observed for nanoparticle-based lithium salts in polymeric matrices[14] and oligomeric solvents.[15,16] In the latter systems, anion immobilization was achieved by grafting the anionic species onto the surface of nanoparticles. For instance, in the experimental system reported by Schaefer et al.,[15] silica nanoparticles were cofunctionalized with polyethylene glycol ligands and tethered anionic species coupled to $Li^+$ ions. When dispersed in a conducting fluid such as tetraglyme, a maximum ionic conductivity of $\sim 10^{-4}$ S/cm was observed at an optimal nanoparticle loading. Interestingly, an order of magnitude increase in conductivity was realized by modifying the tethered anion from $-SO_3^-$ to $-SO_3BF_3^-$.

While the mechanisms underlying ion transport in lithium-salt-doped nanocomposite electrolytes have been examined,[8,11−13] those governing ion transport in the newer class of nanoparticle-based single-ion conducting electrolytes remain poorly understood. Notably, the origins of an optimal nanoparticle loading for (maximizing) ionic conductivity and the pronounced influence that modifying the nanoparticle-tethered counterions has on the magnitude of the conductivity[15] are still unresolved. Further, these properties motivate questions regarding the potential of such materials to conduct alternative cations and the possible avenues for enhancing their ionic conductivity.

In the present study, we use a multiscale simulation approach to understand the mechanisms underlying the conductivity characteristics in single-ion conducting nanoparticle-based electrolytes. We identify the influence of nanoparticle volume fraction, anion and cation choices, and solvent (host) polarity on the ionic conductivity in such systems. Together, our results provide a complete picture for design considerations in single-ion conducting electrolytes based on nanoparticle salts.

**Received:** June 22, 2020
**Accepted:** August 3, 2020
**Published:** August 12, 2020







https://dx.doi.org/10.1021/acs.jpclett.0c01937
J. Phys. Chem. Lett. 2020, 11, 6970−6975

Direct computer simulations of the nanoparticle salt dispersions and their ionic conductivity characteristics using detailed molecular models are computationally intractable. To gain mechanistic insights, we instead adopt a novel approach that uses molecular dynamics (MD) and kinetic Monte Carlo (kMC) simulations to integrate information from length and time scales relevant for ion conduction (Figure 1 and the Supporting Information). At the microscopic scale, we use coarse-grained MD simulations to characterize the spatial distribution of ions and their dynamics in the region between two adjacent functionalized nanoparticles (Figure 1a). At this level, the polymer chains and anions tethered to the nanoparticles, the cations, and oligomeric solvent are all accounted for explicitly. However, we neglect surface curvature effects and model the interparticle region as a confined region between two flat surfaces. The distance between the two surfaces, $L_z$, is varied to model a range of nanoparticle separations. The model parameters were chosen based on the electrolyte system reported by Schaefer et al.[15] Accordingly, both surfaces were grafted with linear polymer chains consisting of 18 beads, each of which represents a single monomer. Similarly, anions were tethered to both surfaces with a grafting density equal to that of the polymer chains. Each solvent molecule was represented as an oligomer with 5 monomer beads. To account for the interaction of ions with the oligomeric solvent and polymer chains, we employ a polymeric Stockmayer model[17−20] in which a freely rotating dipole moment of constant strength $\mu$ is embedded into a finite-size particle, while other bonded and nonbonded interactions are treated using the Kremer−Grest polymer model.[21] The outputs of the MD simulations are used to characterize three features: (i) the effective pair potential $U(r)$ between functionalized spherical nanoparticles, (ii) local cation diffusion coefficients in the direction parallel to the flat surface ($D_{\|}$), and (iii) the spatial distribution of cations in the region between the nanoparticles.

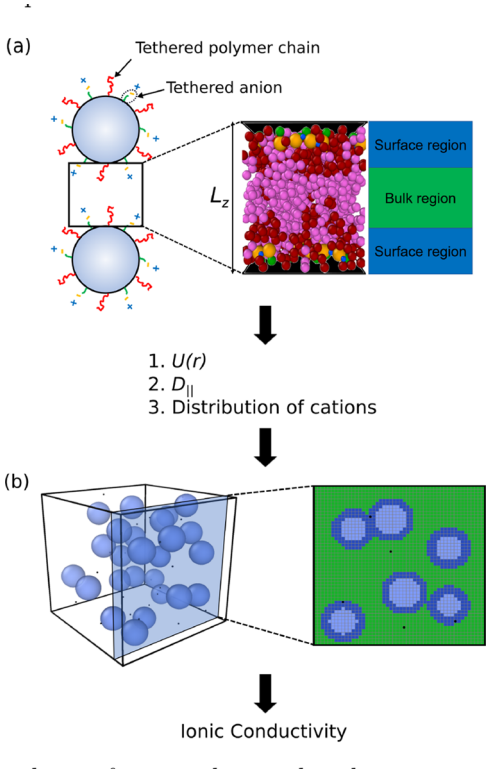


**Figure 1.** Multiscale simulation framework introduced to compute ionic conductivity. (a) Schematic of the MD simulation configuration for the space between adjacent nanoparticles (represented by flat surfaces) and the different spatial regions defined based on the proximity to the nearest nanoparticle surface. (b) Schematic of the multiparticle system with explicit presence of nanoparticles and cations only, including a 2D slice of the 3D on-lattice kMC simulation showing the presence of cations (black tracers) on surface (blue) and bulk (green) sites corresponding to the regions defined in the MD simulations.

At the mesoscopic scale of our simulation framework, on-lattice kMC simulations are used to simulate larger length- and time-scale ion transport in the multiparticle system, adopting a simplified representation which explicitly considers only the nanoparticles and the cations (Figure 1b). Toward this objective, nanoparticle configurations at different bare particle volume fractions $\phi$ (SI Section S2.1) are generated using the effective pair potentials between functionalized nanoparticles (calculated at the microscopic level) and are mapped to an on-lattice representation (SI Section S5.1). As described in SI Section S4.4, information pertaining to the cation spatial distribution and local mobility from the higher-resolution MD simulations are input into the kMC simulations to simulate transport of cations (represented as tracers) on the lattice sites not occupied by the nanoparticles. Because the time scale for diffusion of nanoparticles is long compared to that for cations, we considered the nanoparticles to be immobile. From the

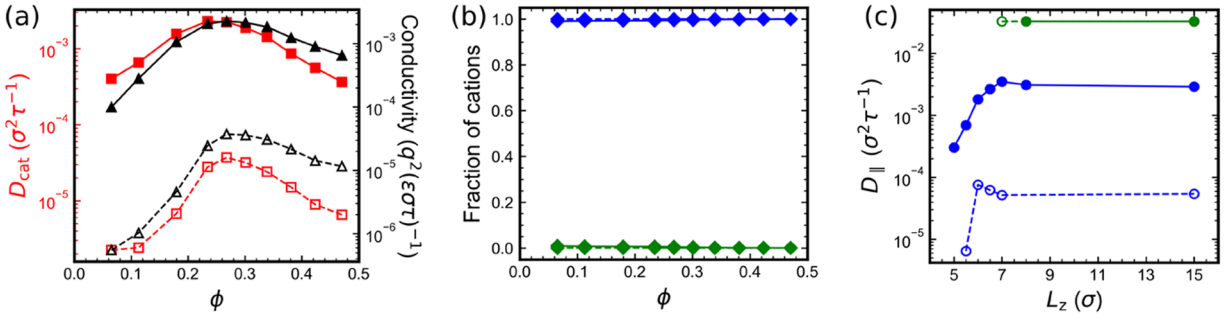


**Figure 2.** Effect of nanoparticle loading and counterion choice on cation transport. (a) Cation diffusivity (red squares) and Nernst−Einstein conductivity (black triangles) as functions of nanoparticle volume fraction. (b) Fraction of cations hosted by the bulk (green diamonds) and surface (blue diamonds) sites at different nanoparticle volume fractions. (c) Local cation diffusivity in the bulk (green circles) and surface (blue circles) regions. Solid and open symbols represent results for larger and smaller anion size, respectively.



https://dx.doi.org/10.1021/acs.jpclett.0c01937
J. Phys. Chem. Lett. 2020, 11, 6970−6975

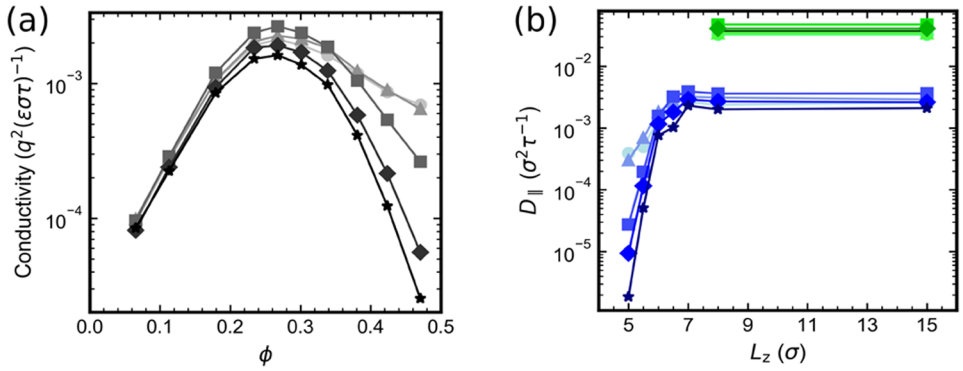


**Figure 3.** Influence of the size of mobile charge carrier on ion transport. (a) Nernst−Einstein conductivity versus nanoparticle volume fraction for different cation sizes. (b) Local cation diffusivities in the bulk (green symbols) and surface (blue symbols) regions for different cation sizes. Different cation sizes are represented as $\sigma_{cat} = 0.25\sigma$ (circles), $0.5\sigma$ (triangles), $0.75\sigma$ (squares), $0.85\sigma$ (diamonds), and $1.0\sigma$ (stars).

resulting cation trajectories of the kMC simulations, the effective cation diffusion coefficient $D_{cat}$ is calculated using the long-time slope of the mean-squared displacement. Because tethering anions to nanoparticle surfaces significantly reduces their mobility, the ionic conductivity $\lambda$ is assumed to be approximately equal to the Nernst−Einstein conductivity $\lambda_{NE}$

$$\lambda \approx \lambda_{NE} = \frac{e^2}{Vk_BT}(N_{cat}z_{cat}^2D_{cat}) \quad (1)$$

where $N_{cat}$ is the number of cations. Because nanoparticles are the only source of cations, $N_{cat}$ is proportional to $\phi$. Complete simulation details and methodology are presented in the SI Sections S1−S3.

Using the multiscale approach described above, and inspired by the experimental results of Schaefer et al.[15] discussed in the introduction, we first probed the influence of anion type and nanoparticle volume fraction on conductivity. Our coarse-grained model distinguishes ions only on the basis of their size, neglecting the specific influence of their chemistry. Accordingly, we consider two different anion sizes, $\sigma_{anion} = 2.0\sigma$ and $1.5\sigma$, where $\sigma$ denotes the size of the monomer both in the polymer chains and in the oligomeric solvent. The cation size ($\sigma_{cat}$) for this set of results was chosen to be $0.5\sigma$ to represent $Li^+$.[18] To mimic poly(ethylene oxide) and tetraglyme as the functionalized polymer chains and oligomeric solvent host,[15,16] the strength of the embedded dipole in their respective monomers was fixed to be that of an ethylene oxide (EO) monomer ($\mu = \mu_{EO}$) at 373 K.

The simulated cation diffusivities in the multiparticle system and the corresponding ionic conductivities display *non-monotonic* dependencies on particle volume fraction (Figure 2a), consistent with the experimental findings of Schaefer et al.[15] These results also qualitatively agree with the reported observation[15] that employing a larger tethered counterion ($-SO_3BF_3^-$) leads to enhanced conductivity relative to a smaller counterion ($-SO_3^-$).

To understand the mechanisms underlying the above results, we quantified the distribution of cations on different site types ("surface" vs "bulk") in the multiparticle system, corresponding to the different types of regions within the space between two nanoparticles (Figure 1a). Explicitly, as illustrated in Figure 1, surface sites represent the region near the nanoparticle where the grafted anions are present, and bulk sites represent the region away from the surface with significant solvent presence.

Irrespective of the anion size considered, the cations are seen to be primarily localized on the surface sites for all particle loadings (Figure 2b). This is a consequence of the strong electrostatic interactions between the cations and the grafted anions. In other words, the primary mechanism of cation diffusion in such nanoparticle-based single-ion conducting electrolytes is by transport along the surface sites. Given this observation, the increase in $D_{cat}$ and conductivity with $\phi$ at low particle loadings can be understood as a consequence of the associated reduction of interparticle distance (SI Section S5.1) and the corresponding increase of connectivity between the surface sites of neighboring particles. This proximity allows for the cations to more easily hop between the surface sites of neighboring particles and traverse larger distances per unit time.[22]

To understand the decrease in conductivity at higher particle volume fractions (Figure 2a), we examine the local cation diffusivities from MD simulations (Figure 2c), which serve as the input for cation hopping rates in the on-lattice kMC model. At higher particle loadings, the nanoparticles approach each other more closely (SI Section S5.1), resulting in an overlap between the surface sites of neighboring particles (see Figure 1b). The cation mobilities in the overlapping surface region are significantly reduced compared to those in the nonoverlapping surface region (Figure 2c). This reduction can be attributed to the combined effect of increased anion−cation electrostatic interactions (SI Section S5.4) and increased steric hindrance effects due to the higher number density of tethered polymer chains and anions in the overlapping surface region (SI Section S1.1). At higher particle loadings, due to significant cation presence on overlapping surface sites (SI Section S5.5), the increased connectivity of surface sites is countered by the slower cation transport in the overlapping surface regions, leading to a decrease in $D_{cat}$ and conductivity with $\phi$. To support this mechanistic interpretation, we repeated the kMC calculations for a fictitious case with $D_{\parallel}$ values in the overlapping surface region set equal to those in the nonoverlapping surface region. Consistent with our hypothesis, $D_{cat}$ does not decrease with $\phi$ at higher particle loadings in such a scenario (SI Section S5.5).

Because cation transport along the surface sites strongly influences $D_{cat}$ at all particle volume fractions, the observed influence of anion size on conductivity (Figure 2a) can be understood based on the corresponding effect it has on $D_{\parallel}$ for cations in the surface region. Specifically, a significant reduction of $D_{\parallel}$ is seen near the surface when smaller (vs


https://dx.doi.org/10.1021/acs.jpclett.0c01937
J. Phys. Chem. Lett. 2020, 11, 6970−6975

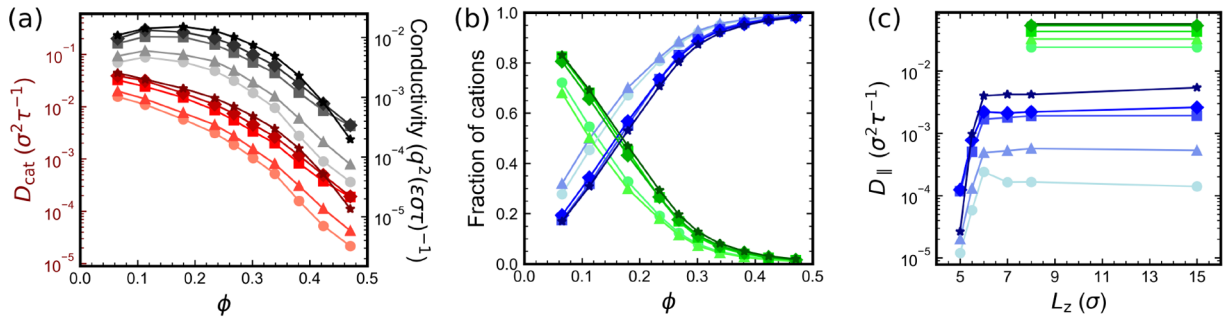


**Figure 4.** Cation transport properties for the high-polarity case ($\mu$ = 2 $\mu_{EO}$). (a) Cation diffusivity (red symbols) and Nernst−Einstein conductivity (black symbols) versus particle volume fraction. (b) Fraction of cations hosted by the bulk (green symbols) and surface (blue symbols) sites at different volume fractions. (c) Local cation diffusivity in the bulk (green symbols) and surface (blue symbols) regions. Different cation sizes are represented as $\sigma_{cat}$ = 0.25$\sigma$ (circles), 0.5$\sigma$ (triangles), 0.75$\sigma$ (squares), 0.85$\sigma$ (diamonds), and 1.0$\sigma$ (stars).

larger) tethered anions are present (Figure 2c), an effect attributable to the stronger ion-pair electrostatic interactions at play in the former case.

The parameters considered for the above results clarify mechanistic underpinnings for the conductivity behavior in nanoparticle-based single-ion conducting electrolytes and help to explain the experimental results reported by Schaefer et al.[15] However, there has also been significant recent interest in developing single-ion conducting batteries based on alkali metals other than Li, such as Na, K, etc.[23−26] These works have further inspired other studies[27−30] which have suggested the size of the mobile charge carrier to be a critical parameter influencing the conductivity. Motivated by such developments, we used our multiscale strategy to predict the influence of mobile cation size on conductivity. To model a range of cation sizes while mimicking the size disparity between $Na^+$, $K^+$, and $Li^+$ ions, we considered four additional cation sizes $\sigma_{cat}$ = 0.25$\sigma$, 0.75$\sigma$, 0.85$\sigma$, and 1.0$\sigma$, while the anion size was fixed to be $\sigma_{anion}$ = 2.0$\sigma$.

The simulation results reveal that there are qualitative differences in the effect that cation size has on conductivity for different nanoparticle volume fractions (Figure 3a). For $\phi$ < 0.3, a nonmonotonic dependence on cation size is observed in which the conductivity first increases and then decreases with increasing cation size. In contrast, for $\phi$ > 0.3, the ionic conductivities are seen to monotonically decrease with increasing cation size. To rationalize these trends, we note that for all the cation sizes considered, the cation distribution on different site types in the multiparticle system (SI Section S5.6) is similar to that noted for $\sigma_{cat}$ = 0.5$\sigma$ (Figure 2b). Accordingly, similar to the arguments presented to explain the results in Figure 2a, the observed conductivity behavior with increasing cation size can be understood based on the corresponding trends for cation mobilities along the nonoverlapping and overlapping surface sites. Explicitly, for $\phi$ < 0.3, most cations are present on the nonoverlapping surface sites (SI Section S5.6) because of the negligible overlap between the surface sites of neighboring particles. From the results in Figure 3b, the cation diffusivities in the nonoverlapping surface region are seen to exhibit a nonmonotonic behavior with increasing cation size, which explains the corresponding conductivity trends. The behavior of cation mobilities in the nonoverlapping surface region can in turn be attributed to the interplay between two competing factors: (a) faster cation transport for larger cations due to weakened ion-pair electrostatic interactions and (b) increased hindrance to the transport of larger cations due to their bulkiness. For $\phi$ > 0.3, with significant overlap between the surface sites of neighboring particles, the conductivity is primarily influenced by the cation diffusivities in the overlapping surface regions. The latter shows a monotonic decrease with cation size (Figure 3b) due to the greater impact of steric hindrance effects compared to ion-pair electrostatic interactions. Such characteristics serve to rationalize the monotonic conductivity behavior at higher nanoparticle loadings.

Given the cation distributions in different regions of the multiparticle systems for all the cases considered (Figure 2b and SI Section S5.6), we infer that the anion−cation electrostatic interactions play a dominant role in localizing the cations near the surface and influencing the ionic conductivities. Considering such findings, we hypothesized that an increase in the fraction of dissociated cations would promote solvent-mediated cation transport and increase the overall conductivity. Such enhanced dissociation can be realized in practice by employing solvent hosts with higher polarities.[18] To test our hypothesis, we considered a system of model oligomeric solvent and nanoparticle-tethered polymeric chains with polarity $\mu$ = 2 $\mu_{EO}$. In this context, we also studied the influence of the cation size while keeping $\sigma_{anion}$ = 2.0$\sigma$.

For low particle loadings ($\phi$ < 0.35), the simulation results show that ionic conductivities for the high-polarity case (Figure 4a) are enhanced compared to those for the low-polarity case (Figure 3a). Further, the nanoparticle composition for maximum conductivity in the high-polarity case is shifted to much lower particle volume fractions compared to that in the low-polarity case. The ionic conductivity is also seen to monotonically increase with cation size for the high-polarity case.

To understand the mechanisms underlying the results displayed in Figure 4a, we turn to the cation distributions in the multiparticle system displayed in Figure 4b. We observe that for the high-polarity case, the cation presence on the bulk sites is significantly enhanced compared to that for the low-polarity case (SI Section S5.6). This redistribution can be understood as a consequence of the stronger electrostatic interactions between the cations and the high-polarity solvent molecules. As a result, we deduce that cation transport through the solvent dictates $D_{cat}$ values for the high-polarity case. Because the cation mobilities through the solvent for the high-polarity case (Figure 4c) are considerably higher than those along the surface for the low-polarity case (Figure 3b), the conductivities are substantially increased by using a high-polarity solvent.



https://dx.doi.org/10.1021/acs.jpclett.0c01937
J. Phys. Chem. Lett. 2020, 11, 6970−6975

To explain the dependence of conductivity on particle volume fraction, we note that with increasing $\phi$, the cation presence in the bulk solvent sites decreases (Figure 4b) because of the increasing number of surface sites. As a consequence, the $D_{cat}$ values exhibit a monotonic decrease with nanoparticle loading. Further, because of the weaker electrostatic interactions between the larger cations and solvent molecules (SI Section S5.7), the local cation diffusivity in the bulk region is seen to increase with increasing cation size (Figure 4c). This explains the corresponding monotonic increase in conductivity with cation size.

In summary, we adopted a multiscale coarse-grained simulation framework to identify the mechanisms underlying the conductivity characteristics for single-ion conducting nanoparticle-based electrolytes. Our results suggest that for the electrolyte systems studied thus far,[15,16] the ionic conductivity is dominated by $Li^+$ transport along nanoparticle surfaces, in the vicinity of the tethered anions. For such cases, the ionic conductivity is influenced by the connectivity of surface transport pathways and the cation diffusivities in the surface region. The latter in turn depends on the strength of anion−cation interaction and the steric hindrance effects on the mobile charge carrier. We further demonstrate that employing high dielectric constant solvents promotes cation transport through the solvent medium and results in elevated conductivity even at relatively lower nanoparticle loadings. Collectively, these mechanistic insights derived from our multiscale simulations provide simple design rules that should prove helpful in the development of nanoparticle-based single-ion conducting electrolytes. In a future study, we plan to explore the influence of other parameters, such as the grafting density of anions, size of the nanoparticles, etc., which are also expected to influence the conductivity of such composites.

## ■ ASSOCIATED CONTENT

### Supporting Information

The Supporting Information is available free of charge at https://pubs.acs.org/doi/10.1021/acs.jpclett.0c01937.

Coarse-grained MD simulation parameters for the region between two nanoparticles (S1.1) and the corresponding force field details (S1.2); model (S2.1) and simulation methodology (S2.2) for generating multiparticle structures; on-lattice kMC simulation details (S3); details of analysis for calculating $D_{||}$ in nonoverlapping surface region (S4.1), overlapping surface region (S4.2), and bulk region (S4.3) and criteria for assigning hopping rates as inputs to kMC model (S4.4); supporting results on the effective pair potential between functionalized nanoparticles and the resulting configurations at different nanoparticle loadings (S5.1), effect of lattice spacing in kMC simulations (S5.2), MSDs of tracer cations from kMC simulations (S5.3), anion−cation coordination for the low-polarity case (S5.4), influence of cation mobilities in the overlapping surface region on $D_{cat}$ values (S5.5), distribution of cations in the multiparticle system for different cation sizes (S5.6), and cation−solvent association autocorrelation functions for the high-polarity case (S5.7) (PDF)

## ■ AUTHOR INFORMATION


### Corresponding Authors

**Thomas M. Truskett** − *McKetta Department of Chemical Engineering and Department of Physics, University of Texas at Austin, Austin, Texas 78712, United States;* orcid.org/0000-0002-6607-6468; Email: truskett@che.utexas.edu

**Venkat Ganesan** − *McKetta Department of Chemical Engineering, University of Texas at Austin, Austin, Texas 78712, United States;* orcid.org/0000-0003-3899-5843; Email: venkat@che.utexas.edu

### Authors

**Sanket Kadulkar** − *McKetta Department of Chemical Engineering, University of Texas at Austin, Austin, Texas 78712, United States;* orcid.org/0000-0002-2834-7677

**Delia J. Milliron** − *McKetta Department of Chemical Engineering, University of Texas at Austin, Austin, Texas 78712, United States;* orcid.org/0000-0002-8737-451X

Complete contact information is available at: https://pubs.acs.org/10.1021/acs.jpclett.0c01937


### Notes

The authors declare no competing financial interest.

## ■ ACKNOWLEDGMENTS

The authors thank Bill Wheatle and Michael P. Howard for valuable discussions. This research was primarily supported by the National Science Foundation through the Center for Dynamics and Control of Materials: an NSF MRSEC under Cooperative Agreement No. DMR-1720595. The authors acknowledge the Texas Advanced Computing Center (TACC) for providing computing resources that have contributed to the research results reported within this Letter. We also acknowledge the Welch Foundation (Grant Nos. F-1599, F-1848, and F-1696) for support.

## ■ REFERENCES


(1) Xu, K. Electrolytes and Interphases in Li-Ion Batteries and Beyond. *Chem. Rev.* **2014**, *114*, 11503−11618.

(2) Li, Q.; Chen, J.; Fan, L.; Kong, X.; Lu, Y. Progress in electrolytes for rechargeable Li-based batteries and beyond. *Green Energy Environ* **2016**, *1*, 18−42.

(3) Diederichsen, K. M.; McShane, E. J.; McCloskey, B. D. Promising Routes to a High Li + Transference Number Electrolyte for Lithium Ion Batteries. *ACS Energy Lett.* **2017**, *2*, 2563−2575.

(4) Chazalviel, J.-N. Electrochemical aspects of the generation of ramified metallic electrodeposits. *Phys. Rev. A: At., Mol., Opt. Phys.* **1990**, *42*, 7355−7367.

(5) Armand, M.; Tarascon, J.-M. Building better batteries. *Nature* **2008**, *451*, 652−657.

(6) Capiglia, C.; Mustarelli, P.; Quartarone, E.; Tomasi, C.; Magistris, A. Effects of nanoscale $SiO_2$ on the thermal and transport properties of solvent-free, poly(ethylene oxide) (PEO)-based polymer electrolytes. *Solid State Ionics* **1999**, *118*, 73−79.

(7) Croce, F.; Settimi, L.; Scrosati, B. Superacid $ZrO_2$-added, composite polymer electrolytes with improved transport properties. *Electrochem. Commun.* **2006**, *8*, 364−368.

(8) Croce, F.; Appetecchi, G. B.; Persi, L.; Scrosati, B. Nanocomposite polymer electrolytes for lithium batteries. *Nature* **1998**, *394*, 456−458.

(9) Xiong, H. M.; Zhao, X.; Chen, J. S. New Polymer-Inorganic Nanocomposites: PEO − ZnO and PEO − ZnO − $LiClO_4$ Films. *J. Phys. Chem. B* **2001**, *105*, 10169−10174.

(10) Austin Suthanthiraraj, S.; Johnsi, M. Nanocomposite polymer electrolytes. *Ionics* **2017**, *23*, 2531−2542.

(11) Croce, F.; Persi, L.; Scrosati, B.; Serraino-Fiory, F.; Plichta, E.; Hendrickson, M. A. Role of the ceramic fillers in enhancing the transport properties of composite polymer electrolytes. *Electrochim. Acta* **2001**, *46*, 2457−2461.
(12) Croce, F.; Curini, R.; Martinelli, A.; Persi, L.; Ronci, F.; Scrosati, B.; Caminiti, R. Physical and Chemical Properties of Nanocomposite Polymer Electrolytes. *J. Phys. Chem. B* **1999**, *103*, 10632−10638.
(13) D'Epifanio, A.; Serraino Fiory, F.; Licoccia, S.; Traversa, E.; Scrosati, B.; Croce, F. Metallic-lithium, $LiFePO_4$-based polymer battery using PEO−$ZrO_2$ nanocomposite polymer electrolyte. *J. Appl. Electrochem.* **2004**, *34*, 403−408.
(14) Bertasi, F.; Vezzù, K.; Giffin, G. A.; Nosach, T.; Sideris, P.; Greenbaum, S.; Vittadello, M.; Di Noto, V. Single-ion-conducting nanocomposite polymer electrolytes based on PEG400 and anionic nanoparticles: Part 2. Electrical characterization. *Int. J. Hydrogen Energy* **2014**, *39*, 2884−2895.
(15) Schaefer, J. L.; Yanga, D. A.; Archer, L. A. High Lithium Transference Number Electrolytes via Creation of 3-Dimensional, Charged, Nanoporous Networks from Dense Functionalized Nanoparticle Composites. *Chem. Mater.* **2013**, *25*, 834−839.
(16) Zhao, H.; Jia, Z.; Yuan, W.; Hu, H.; Fu, Y.; Baker, G. L.; Liu, G. Fumed Silica-Based Single-Ion Nanocomposite Electrolyte for Lithium Batteries. *ACS Appl. Mater. Interfaces* **2015**, *7*, 19335−19341.
(17) Liu, L.; Nakamura, I. Solvation Energy of Ions in Polymers: Effects of Chain Length and Connectivity on Saturated Dipoles near Ions. *J. Phys. Chem. B* **2017**, *121*, 3142−3150.
(18) Wheatle, B. K.; Lynd, N. A.; Ganesan, V. Effect of Polymer Polarity on Ion Transport: A Competition between Ion Aggregation and Polymer Segmental Dynamics. *ACS Macro Lett.* **2018**, *7*, 1149−1154.
(19) Wheatle, B. K.; Fuentes, E. F.; Lynd, N. A.; Ganesan, V. Influence of Host Polarity on Correlating Salt Concentration, Molecular Weight, and Molar Conductivity in Polymer Electrolytes. *ACS Macro Lett.* **2019**, *8*, 888−892.
(20) Wheatle, B. K.; Lynd, N. A.; Ganesan, V. Effect of Host Incompatibility and Polarity Contrast on Ion Transport in Ternary Polymer-Polymer-Salt Blend Electrolytes. *Macromolecules* **2020**, *53*, 875−884.
(21) Kremer, K.; Grest, G. S. Dynamics of entangled linear polymer melts: A molecular-dynamics simulation. *J. Chem. Phys.* **1990**, *92*, 5057−5086.
(22) Kadulkar, S.; Banerjee, D.; Khabaz, F.; Bonnecaze, R. T.; Truskett, T. M.; Ganesan, V. Influence of morphology of colloidal nanoparticle gels on ion transport and rheology. *J. Chem. Phys.* **2019**, *150*, 214903.
(23) Furukawa, T.; Yoneya, K.; Takahashi, Y.; Ito, K.; Ohno, H. Correlation between ionic and dipolar motions in a single-ion conducting polymer P[$MEO_9$-MAM]. *Electrochim. Acta* **2000**, *45*, 1443−1448.
(24) Pan, Q.; Li, Z.; Zhang, W.; Zeng, D.; Sun, Y.; Cheng, H. Single ion conducting sodium ion batteries enabled by a sodium ion exchanged poly(bis(4-carbonyl benzene sulfonyl)imide-*co*-2,5-diamino benzesulfonic acid) polymer electrolyte. *Solid State Ionics* **2017**, *300*, 60−66.
(25) Elmore, T. C.; Seidler, E. M.; Ford, O. H.; Merrill, C. L.; Upadhyay, P. S.; Schneider, F. W.; Schaefer, L. J. Ion Transport in Solvent-Free, Crosslinked, Single-Ion Conducting Polymer Electrolytes for Post-Lithium Ion Batteries. *Batteries* **2018**, *4*, 28.
(26) Cao, C.; Liu, W.; Tan, L.; Liao, X.; Li, L. Sodium-ion batteries using ion exchange membranes as electrolytes and separators. *Chem. Commun.* **2013**, *49*, 11740−11742.
(27) Keith, J. R.; Rebello, N. J.; Cowen, B. J.; Ganesan, V. Influence of Counterion Structure on Conductivity of Polymerized Ionic Liquids. *ACS Macro Lett.* **2019**, *8*, 387−392.
(28) Griffin, P. J.; Freyer, J. L.; Han, N.; Geller, N.; Yin, X.; Gheewala, C. D.; Lambert, T. H.; Campos, L. M.; Winey, K. I. Ion Transport in Cyclopropenium-Based Polymerized Ionic Liquids. *Macromolecules* **2018**, *51*, 1681−1687.
(29) Paren, B. A.; Raghunathan, R.; Knudson, I. J.; Freyer, J. L.; Campos, L. M.; Winey, K. I. Impact of building block structure on ion transport in cyclopropenium-based polymerized ionic liquids. *Polym. Chem.* **2019**, *10*, 2832−2839.
(30) Ma, B.; Nguyen, T. D.; Olvera de la Cruz, M. Control of Ionic Mobility via Charge Size Asymmetry in Random Ionomers. *Nano Lett.* **2020**, *20*, 43−49.


https://dx.doi.org/10.1021/acs.jpclett.0c01937
*J. Phys. Chem. Lett.* 2020, 11, 6970−6975